

Structural and spin transitions in Fe_2O_3

Dipta Bhanu Ghosh, and Stefano de Gironcoli

DEMOCRITOS National Simulation Center, Trieste 34014, Italy

SISSA – Scuola Internazionale Superiore di Studi Avanzati, Trieste 34014, Italy

(Dated: March 12, 2009)

First principles density functional calculations for Fe_2O_3 has been performed over a wide range of pressures. The ground state is corundum-type hematite and is an antiferromagnetic insulator. This is in good agreement with experiment and other theoretical studies. On increasing pressure, the ground-state high-spin magnetic phase transforms to low spin via the closure of the charge transfer gap. The system also evolves to a new orthorhombic structure. Distorted corundum or $\text{Rh}_2\text{O}_3(\text{II})$ type structure with Pbcn symmetry and Pbnm type perovskite structure are two known competitive candidates for this structural phase, based on *single*-cationic type and *two*-cationic type picture, respectively. In our calculations, at about 38 GPa, $\text{Rh}_2\text{O}_3(\text{II})$ type structure becomes more stable with respect to the ground state hematite. Relative stability of Pbnm type perovskite is ruled out by our calculations in this pressure regime. The $\text{Rh}_2\text{O}_3(\text{II})$ type structure remains in its low spin state, with $1 \mu_B/\text{Fe}$ atom, up to about 120 GPa. At this pressure the nonmagnetic solution in $\text{Rh}_2\text{O}_3(\text{II})$ type structure becomes more favorable with respect to the low spin one. By further increasing the pressure at about 330 GPa, the system evolves to yet another new structural phase. This new orthorhombic structural phase is nonmagnetic and has Pmc2₁ symmetry, a subgroup of Cmc₂. Surprisingly, on furthering rising the pressure, a Pbnm type nonmagnetic solution becomes competitive with the Pmc2₁ type structure and finally becomes stable at about 880 GPa.

PACS numbers:

I. INTRODUCTION

Iron (Fe), one of the most abundant element on earth, is believed to contribute significantly to the mantle core characteristics in pure oxide form (FeO , Fe_2O_3) or in mixed oxide forms such as $(\text{Mg,Fe})\text{O}$ and $(\text{Mg,Fe})\text{SiO}_3$. Of these oxides, Fe_2O_3 shows versatility in its structural, magnetic and electronic properties. The ambient pressure phase $\alpha\text{-Fe}_2\text{O}_3$ (hematite) is corundum-type and is a wide-gap antiferromagnetic insulator¹. It becomes weakly ferromagnetic between Morin temperature, T_M ($=260$ K), and Néel temperature, T_N ($=955$ K), as a result of the canting of the spins of the two sublattices.

Owing to its diverse intriguing properties it drew a significant amount of attention in the scientific community from the sixties. Reid and Ringwood² based on McQueen and Marsh's shock-wave experiment³ proposed a new (denser) structural phase to exist between 60 – 120 GPa. In the subsequent years the onset of an high pressure phase at ~ 50 GPa was confirmed by quite a few studies^{4,5,6,7}. However, there was ambiguity concerning the crystal structure of the new phase. While Shannon *et. al.*⁴ opted for the distorted corundum ($\text{Rh}_2\text{O}_3(\text{II})$) structure speculating on a single cationic nature of Fe, *i.e.* Fe^{3+} , the group of Suzuki *et. al.*⁶ went with the idea of orthorhombic perovskite structure with ABO_3 formula with a *two*-type of cationic Fe (Fe^{2+} and Fe^{4+}) picture. Room temperature Mössbauer spectroscopy (MS) experiments^{6,8,9} revealed a non magnetic component at ~ 50 GPa, coexisting with the magnetic phase. A volume collapse of $\sim 10\%$, concurrent with the onset of the phase transition at ~ 50 GPa, corroborating a first order phase transition, was observed by Olsen *et. al.*⁷. Assuming the two cationic type picture this volume collapse was quali-

tatively explained by the increase in coordination number (from 6 to 8) in one of the Fe sites.

To resolve the issue of *one* or *two*-cationic types and correlate/separate the spin and structural transitions a number of investigations have been done in the more recent years. Of them, X-ray diffraction (XRD), MS at 300K and electrical resistivity measurements by Pasternak *et. al.*¹⁰ unequivocally assigned high pressure structural phase as the nonmagnetic distorted corundum or $\text{Rh}_2\text{O}_3(\text{II})$ type. They explained the intermediate region between the insulating and metallic region in their electrical resistivity data qualitatively by the coexistence of the insulating corundum phase (denoted HP1 from now on) with the metallic $\text{Rh}_2\text{O}_3(\text{II})$ (denoted HP2 in the following).

Other XRD and X-ray emission spectroscopy (XES) experiments by Badro *et. al.*¹¹ could separate the electronic transition from the crystallographic transition. From their XES data it was concluded that the high spin (HS) could be stabilized in the high pressure structural phase, *i.e.* in HP2 phase, at low temperatures. At high temperatures, however, the low spin (LS) state of HP2 is stable. That this LS state is a weakly paramagnetic one was concluded by the presence of a satellite ($K\beta'$) in the XES spectra.¹¹

The room temperature Raman spectroscopy study by Shim and Duffy¹² found the upper boundary for this phase transition (where no HP1 signal is left) to be between 54 – 56 GPa on compression. While decompressing, however, some (frequency) modes of the HP2 phase survive down to 25 GPa. The combined experimental and theoretical study by Rozenberg *et. al.*¹³ also reported of the sluggishness in the transition from HP1 to HP2. The onset of high pressure phase start at about ~ 40 GPa

and at 76 GPa they could find only the components of the high pressure phase. Their theoretical calculations at 76 GPa predict the stability of the $\text{Rh}_2\text{O}_3(\text{II})$ (*i.e.* HP2) phase with respect to the orthorhombic perovskite phase (*opv* in the following).

The XRD study by Ono *et al.*^{14,15} suggested that high temperature heating has a major role to play in controlling the phase transition pressure. The phase transition pressure of $\sim 45 - 50$ GPa at room temperature drops down by about $15 - 20$ GPa when the samples are heated to overcome the kinetic barriers hindering the transition. Their estimated transition pressure was ~ 26.2 GPa at 300K. However, in this study they were not conclusive about the crystal structure of the high pressure phase.

There are a few theoretical studies of the Fe_2O_3 system in the hematite phase.^{16,17,18,19} To the best of our knowledge, however, there are no theoretical studies concerning the low and high pressures phases and their stabilities. Neither the issue of transition from HS to LS is addressed. In this work we will shed light on these issues of the Fe_2O_3 system from first principles approach, based on density functional theory (DFT).

The paper is organized as follows: after a brief discussion of the calculational details we will proceed to the next sections dealing with the results of our calculations. We will start with the ambient pressure phase, $\alpha\text{-Fe}_2\text{O}_3$ at the GGA level. After that we will proceed with two (orthorhombic perovskite, Pbnm type and $\text{Rh}_2\text{O}_3(\text{II})$, Pbcn type) competing candidate structures for the high-pressure phase following the hematite one. The next subsection will focus on the theoretical search for the experimentally found, but structurally unresolved, post-perovskite type phase. At the end we will comment on the nature of the spin transition and the evolution of the structure.

II. CALCULATIONAL DETAILS

We have performed first-principles density functional calculations to analyze the spin and structural transitions in Fe_2O_3 . Calculations were performed using the PBE generalized gradient approximation (GGA)²⁰. Variable-cell-shape molecular dynamics²¹ was used for the full structural optimization at arbitrary pressures. Eight electrons ($3d^7 4s^1$) per Fe atom and six electrons ($2s^2 2p^4$) per O atom were taken in the valence in the generation of the ultrasoft pseudopotential within the scheme of Rabe Rappe Kaxiras Joannopoulos ultrasoft pseudopotential²². Total energy convergence of the wave function cut-off and kinetic energy cut-off (for the charge density) were checked. And the final values used were 35 and 380 Ryd, respectively. The Brillouin zone integration was performed using a Monkhorst and Pack²³ mesh of $6 \times 6 \times 6$ points. For the HP1 phase (corundum structure) we used the rhombohedral cell consisting of 2 formula units (*f.u.*) of Fe_2O_3 . For the HP2 phase, and possible HP3/HP4 phase, orthorhombic cell consisting of

4 *f.u.* of Fe_2O_3 were used.

III. RESULTS AND DISCUSSIONS

A. hematite

In the elemental rhombohedral cell, reported in Fig. 1, four Fe atoms, spread along the z-axis, are grouped into two sets: two Fe (B-C) atoms at a shorter distance, denoted by $(\text{Fe-Fe})_{\text{short}}$ and a pair (A-B or C-D) at a larger distance, denoted by $(\text{Fe-Fe})_{\text{long}}$. Depending on the orientations of the magnetization of the different Fe atoms, there can be four possible magnetic configurations ($\text{AF1} \equiv \text{ABCD} :: ++--$, $\text{AF2} \equiv \text{ABCD} :: +-+-$, $\text{AF3} \equiv \text{ABCD} :: -+ -+$ and $\text{FM} \equiv \text{ABCD} :: ++++$, where + and - correspond to opposite magnetization directions). The optimized lattice parameters as extracted from energy-volume curves are 10.277, 10.317, 10.340, 10.355 *a.u.* respectively for the AF1, AF2, AF3 and FM configurations. The most stable magnetic configuration is AF1, as can be seen from the curves in Fig. 1. These lattice parameters were then used as the starting point for the subsequent cell optimization at finite pressures. In all antiferromagnetic configurations the Fe magnetic moments are close to $3.8 \mu_B/\text{atom}$ at 0 GPa. Moreover all antiferromagnetic solutions are insulating while the ferromagnetic solution is metallic.

The partial density of states at 0 GPa, for AF1, is shown in the lowest panel of Fig. 2. From the figure it is evident that the top of the valence band is occupied by the $2p$ states of O and the $3d$ states of Fe on an equal basis. The valence and conduction band edges are separated by a well defined gap of about 0.3 eV. It is to be noted that, all the antiferromagnetic configurations show a similar valence and conduction edges, with similar value of the fundamental gap, while the FM configuration is metallic. The experimental scenario is a bit different: the top of the valence band has mainly O- $2p$ character, and the experimental value of the band gap is 2.0 eV [24]. Both these deficiencies can be attributed to an incomplete treatment of electronic correlation at the LDA or GGA level. Similar results have been reported earlier and, for instance, the calculated values of the band gap is 0.3 eV by employing pseudopotential¹⁶, 0.75 eV by augmented spherical wave method¹⁸ and 0.51 eV by linear muffin-tin orbital¹⁷, respectively. The band gap value in a Hartree Fock calculation¹⁹ is instead of grossly overestimated as 11 eV due to the complete neglect of correlation effects. A good representation of the band gap and of the atomic decomposition of the band edge states can be obtained by including strong correlation effects via $\text{GGA} + U$, as can be seen in the upper panels of Fig. 2. We wish to emphasize here, however, the qualitative agreement of the GGA results with experiments of the basic electronic structure of hematite.

To check the relative stability of the different magnetic configurations at finite pressures we have calculated their

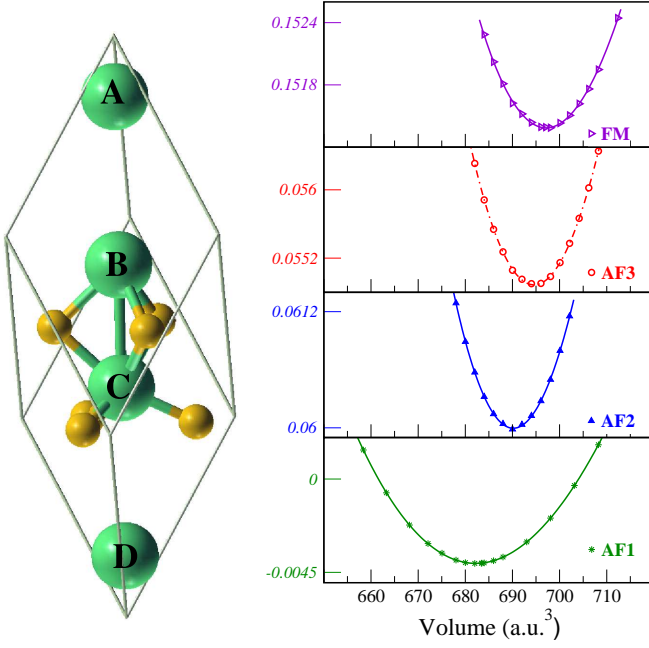


FIG. 1: (color online) Left panel: The rhombohedral unit cell of Fe_2O_3 . The (big) green balls correspond to Fe atoms and brown ones correspond to Oxygen atoms. Right panel: Energy-Volume curves (symbols correspond to calculated data and the curves are fits to data obtained using Murnaghan's equation of state) for the four magnetic configurations of hematite considered in this work. Note that the curve corresponding to AF1 configuration (see text for notation) has the lowest energy at the minimum and is therefore the ground state configuration.

enthalpies by fully optimizing each of the structures by variable-cell damped dynamics at several pressures. The results are collected in Figure. 3

B. spin transition

As can be seen in Fig. 3(a), for all the magnetic phases the value of the magnetic moment per Fe atom remains almost constant at about $3.8 \mu_B/\text{Fe}$ atom at low pressure (large volumes). With decreasing volume (increasing pressure) there is a sudden collapse in magnetic moment magnitude to $\sim 1 \mu_B/\text{Fe}$ atom.

The relative enthalpy curves of HS and LS phases for the various configurations are depicted in Fig. 3(b). The crossover from the HS to LS occurs at around 36, 24.5 and 19.5 GPa, for the AF1, AF2, AF3 configurations, respectively, and at ~ 5 GPa for the FM (not shown in the figure). From this figure it is clear that the AF1 configuration is the most stable one upto a pressure of about 34 GPa, where the FM phase becomes more stable. This trend was also observed by Rollman et.al.¹⁶ Overall, the computed sequence of relative stability of the different magnetic phases of hematite is in agreement with exper-

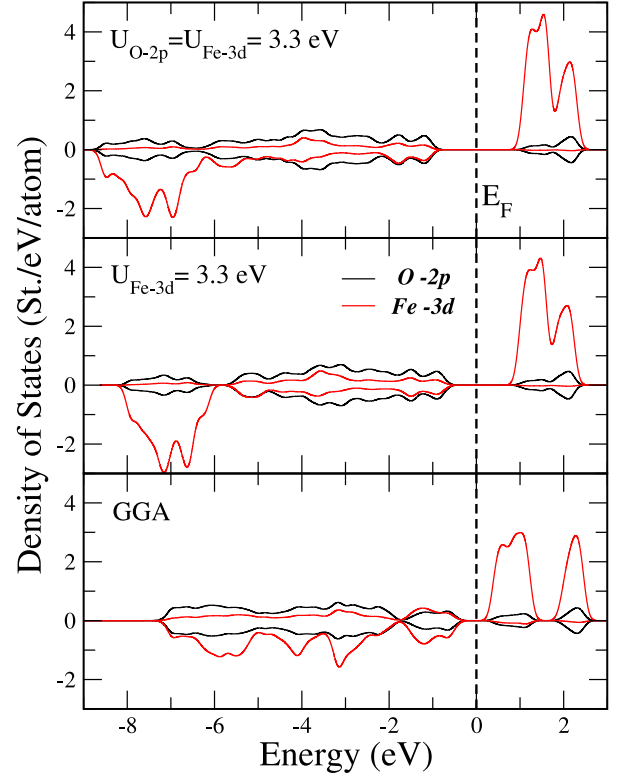


FIG. 2: (color online) Projected Density of States for the hematite (AF1) at 0 GPa per atom for GGA and GGA + U calculations.

iment and previous calculations.^{16,18}

This HS-LS spin collapse at the transition is also accompanied by a sudden change in the magnitude of a number of inter- and intra- octahedral structural parameters. Notable inter-octahedral structural parameters are the $(\text{Fe}-\text{Fe})_{\text{short}}$ and $(\text{Fe}-\text{Fe})_{\text{long}}$ distances, which decrease and increase, respectively, at the spin transition as can be seen from Table I. The same was observed by Rollman et.al.¹⁶ in their GGA calculations.

Although also the remote surroundings (*i.e.* the next to next-nearest neighbors and inter-octahedral distances) have non-negligible effects on the nature of the spin transition, the most significant changes observed at the transition concern mainly the octahedra, as already pointed out by a number of studies.^{25,26,27,28,29,30,31} Of the intra-octahedral structural parameters, the average Fe-O bond lengths, as shown in Fig. 3(c), show a jump from higher to lower values and display two very distinct and well separated slopes in the HS and in the LS configurations.

Two other intra-octahedral structural parameters that displays significant changes at the transition are the Fe-O bond-length distortion and the octahedral-angle variance. Fe-O bond-length distortion, $\delta d_{\text{Fe-O}}$, is defined as $\delta d_{\text{Fe-O}} = \frac{1}{D} \sum_{i=1}^6 |\Delta d_i|$, where D is the average (octa-

TABLE I: Variation of Fe-Fe bond lengths and of the average Fe-O bond lengths in the octahedral coordination across the spin transition. Increases (\uparrow) and decreases (\downarrow) in bond lengths are marked by arrows. The values of the distortion index, δd_{Fe-O} , and of the octahedral angle variance, $\Delta\theta$, at the transition are also reported.

	$(Fe-Fe)_{short}$ (\AA) \downarrow	$(Fe-Fe)_{long}$ (\AA) \uparrow	$(Fe-O)$ (\AA) \downarrow	δd_{Fe-O}	$\Delta\theta^2$ (deg. ²)
Hematite:					
AF1	2.725 - 2.525	3.792 - 4.043	1.929 - 1.867	0.0427 - 0.0248	77.8 - 34.0
AF2	2.787 - 2.508	3.786 - 3.946	1.959 - 1.883	0.0298 - 0.0234	85.2 - 36.5
AF3	2.730 - 2.559	3.826 - 4.077	1.976 - 1.892	0.0480 - 0.0246	81.0 - 35.8

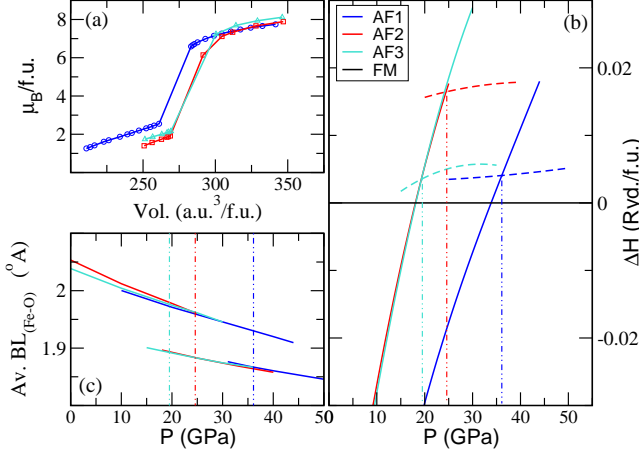


FIG. 3: (color online) Results for the different magnetic configurations in the hematite structure. (a) Magnetic moment as a function of volume calculated at the GGA level. (b) Relative enthalpy curves. Solid lines (vertical) correspond to high spin (HS) and dashed lines (horizontal) are for low (LS: $1\mu_B/\text{Fe}$ atom) spins. The reference enthalpy (base line) corresponds to the FM configuration in the LS phase. (c) Dependence of the average Fe-O bond-length (in the octahedra) with pressure. Vertical dotted lines correspond to the spin transition pressures for different magnetic configurations. For the FM configuration, not shown in figure, similar characteristics are observed but at much smaller pressure of around 5 GPa.

hedral) Fe-O bond-length at that particular volume and Δd_i is the difference of the i -th Fe-O bond-length from its average. The octahedral-angle variance³² is instead given by $\Delta\theta^2 = \sum_{j=1}^{12} (\theta_j - 90)^2 / 11$. Where θ_j is the variation of the j -th O-Fe-O angle from its ideal value of 90° .

At the spin transition, both the mentioned intra-octahedral structural parameters, δd_{Fe-O} and $\Delta\theta^2$, show a jump from a larger to a smaller value as can be seen from Table. I. This indicates that at the spin transition the octahedra become more regular and this happens irrespective of the octahedral surroundings.³³ Moreover, the sudden jump of these parameters can directly be related with the $\sim 10\%$ volume collapse that is observed for all the magnetic phases at the spin transition.

C. structural transition

Along with the spin transition discussed above, $\alpha\text{-Fe}_2\text{O}_3$ also undergoes structural phase transition/s under pressure and temperature. Two candidate structures for this phase are the orthorhombic perovskite (*opv*) with *Pbnm* symmetry and the $\text{Rh}_2\text{O}_3(\text{II})$ with *Pbcn* symmetry.

In hematite ($\alpha\text{-Fe}_2\text{O}_3$), in the corundum structure, the Fe atoms sit inside the cage of a single kind of polyhedra which are octahedra. Each of these octahedra shares three edges and one face with the neighbouring octahedra. $\text{Rh}_2\text{O}_3(\text{II})$ structure with *Pbcn* symmetry is of the distorted corundum type and also has the same single type octahedral arrangement. Owing to a larger octahedral distortion and rotation of the octahedra in $\text{Rh}_2\text{O}_3(\text{II})$, one of the three sharing edges is broken by the alteration of one of the coordinating oxygens. This crystallographic change is minor as can be seen from the Fig. 4: instead of three shared edges as in hematite, octahedra in $\text{Rh}_2\text{O}_3(\text{II})$ have two sharing edges with the addition of a corner sharing bonding.

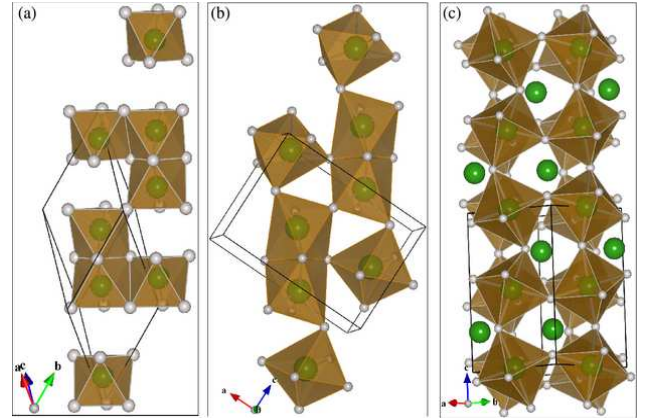


FIG. 4: (color online) Polyhedral structures of Fe_2O_3 in different crystal packing. (a): hematite, (b): $\text{Rh}_2\text{O}_3(\text{II})$, (c): *Pbnm* type perovskite. Small white spheres are oxygen atoms and big green ones are for the Fe atoms.

On the other hand, for the perovskite structure with *Pbnm* symmetry, there are two types of polyhedral environment surrounding Fe atoms. The six-fold coordinated (octahedra) and the 8-fold coordinated polyhedra

are arranged in alternate layers along the z direction. The octahedral connectivity is via corner sharing, while the 8-fold coordinated polyhedra are connected to each other by edge and corner sharing. The interpolyhedral connectivity (between octahedra and 8-fold coordinated polyhedra) is maintained via face and edge sharing.

A Mössbauer spectroscopy study at 300K by Pasternak *et. al.*¹⁰ showed that the transition from hematite to the high-pressure phase starts at about 45 GPa and completes at about 72 GPa. The existence of *opv* phase at high-pressure was ruled out by pointing out the single cationic nature of the Fe-ions. Moreover, Fe-ions were characterized as non-magnetic and the magnetic to non-magnetic transition connected to the structural phase transition. In a later study Badro *et. al.*¹¹ could separate the crystallographic transition from the spin transition. According to this study the spin transition is isostructural and takes place in the high-pressure phase. In a more recent study Ono *et. al.*^{14,15} reported the transition pressure to be 26.2 GPa at 300 K. It was concluded there that high-temperature heating played a fundamental role in overcoming the kinetic barrier hindering the phase transition, thus lowering the transition pressure. The combined experimental and theoretical study by Rozenberg *et. al.*¹³ also indicated $\text{Rh}_2\text{O}_3(\text{II})$ as the HP2 phase. The *opv* phase was found to be higher in energy than the $\text{Rh}_2\text{O}_3(\text{II})$ phase by as much as 25 Ryd/f.u. at 76 GPa. However, no other detailed theoretical study exist on the relative stability of these two phases.

We have calculated the static enthalpies for these two structures, both in FM and AF configurations, for a finite range of pressures. Fig. 5 shows the relative enthalpy-pressure curves for these two candidate structures along with the AF1 corundum structure. As can be seen from the figure, at low pressures all structures show an HS solution. Corundum in the HS AF1 configuration is the most stable one upto about 34 GPa. At this pressure the enthalpy of corundum in the LS FM configuration becomes lower. This crossover from HS AF to LS FM is also observed for $\text{Rh}_2\text{O}_3(\text{II})$ structure at about 26 GPa (as can be seen from the crossing of the *HP2-af-hs* and *HP2-fm-ls* curves in Fig. 5). The crossover from HS to LS is also present for *opv* structure, but only in the octahedral sites. The 8-fold coordinated polyhedra remain in the high spin and hence, overall, the system remain in a kind of intermediate mixed (half HS and half LS) spin state. We mention also that from ~ 34 GPa to about 38 GPa the LS FM configuration in the corundum structure is the most stable one. After this, in the broad range of pressure from ~ 38 GPa to almost 120 GPa the $\text{Rh}_2\text{O}_3(\text{II})$ structure in the LS FM configuration is the most stable. With increasing pressure there is a gradual decrease of magnetization in the system that finally becomes non-magnetic from ~ 120 GPa onwards. Hence, upto the pressure range shown in this figure, *opv* does not have any stability region. Therefore, our calculations, in agreement with recent experiments,^{10,11,16} rule out the two cationic site picture, *i.e.* *opv*, and estab-

lishes $\text{Rh}_2\text{O}_3(\text{II})$ as the HP2 or next stable phase after the corundum one..

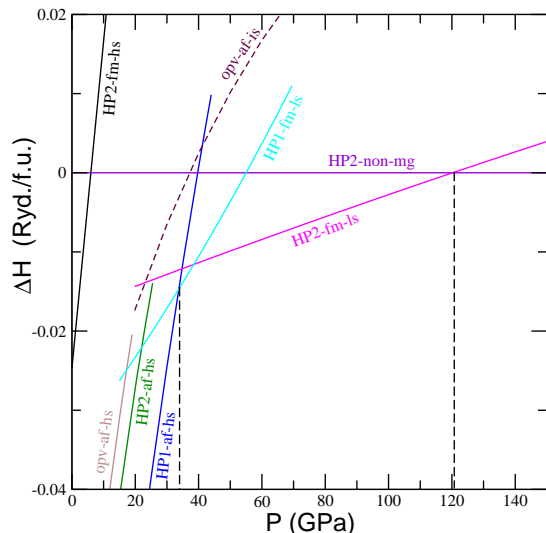


FIG. 5: (color online) Relative enthalpy curves for the $\text{Rh}_2\text{O}_3(\text{II})$ (HP2), *opv* (*opv*) along with the corundum structure (HP1). HP1 structure in the LS phase is dynamically stable upto about 180 GPa. For the *opv* structure in the FM configuration, not shown here, the relative enthalpy curve remain well above the base line here. The dashed vertical lines are guide to the eye to locate the transition pressures.

D. further structural transitions

The high temperature experiments by Ono *et. al.*¹⁴ reported of another structural phase transition after the HP2 phase. Their data show that the transformation of this phase begins at around 60 GPa and 2500K. They identified this phase as CaIrO_3 type with Cmcm symmetry. However, this designation was made without a detailed structural analysis in analogy to other systems. The prototype sesquioxide, Al_2O_3 , for instance, having corundum structure at ambient conditions, undergoes a structural transformation from $\text{Rh}_2\text{O}_3(\text{II})$ type phase to a post-perovskite one of CaIrO_3 type, and this structure has been found as the post-perovskite phase in most of the instances of post-perovskite phases discovered till today [see Ref.³⁴ and references therein].

In Fe_2O_3 , being another sesquioxide, it is therefore natural to explore the possible higher pressure phases starting with CaIrO_3 structure with Cmcm symmetry (denoted as HP3 from here). In terms of polyhedral arrangements this structure has two types of polyhedral arrangements, *i.e.* octahedra and 8-fold coordinated polyhedra. The difference with respect to the Pbnm type structure is that there is no longer any inter-layer octahedral connection. Instead alternate layers of octahedra and 8-fold coordinated polyhedra form the structure as shown in Fig. 6(a).

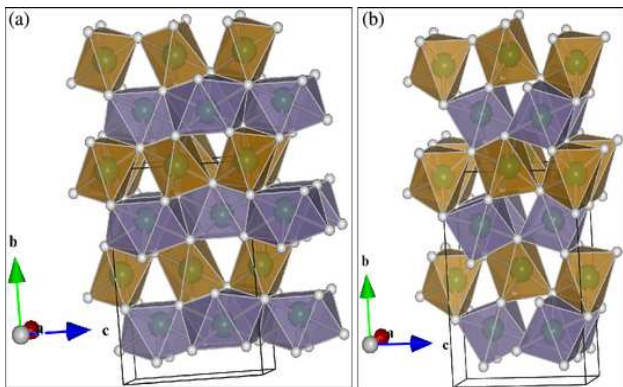


FIG. 6: (color online) Two candidate high pressure structures of Fe₂O₃. (a) HP3: Cmc type post-perovskite and (b) HP4: Pmc₂₁ type post-perovskite. Small white spheres are oxygen atoms and big green ones are for the Fe atoms.

In Fig. 7, one can see that around 200 GPa both *opv* and the HP3 phases are in the intermediate spin state (Fe in the octahedral cage is in low spin state, while it is in a high-spin state when 8-fold coordinated to Oxygen) and are dynamically stable. However, upto about 337 GPa, the enthalpy of the nonmagnetic HP2 phase is lower. From 337 GPa onwards, the enthalpy of the nonmagnetic phase of a new structure³⁵ crosses the HP2 one. This new structure, denoted HP4 in the following, has Pmc₂₁ symmetry with an orthorhombic unit cell consisting of 20 atoms. Pmc₂₁ is a subgroup of Cmc. The 4c,4a and 8f Wyckoff positions in Cmc are split into 2a and 2b Wyckoff positions in Pmc₂₁ space group. This splitting of the symmetry positions leads to different kind of polyhedral arrangement in the new phase. Instead of alternate layers of octahedra and of 8-fold coordinated polyhedra as in Cmc, the arrangement in Pmc₂₁ corresponds to alternate layers of octahedra and of 7-fold coordinated polyhedra. Comparing HP4 with HP3, it can be seen from Fig. 7 that the AF HP3 curve, labelled *HP3-af-is*, crosses the non-magnetic HP4 curve (*HP4-non-mg*) at ~ 225 GPa. This newly achieved structural phase (HP4) remains stable for a wide pressure range. At much higher pressures, however, the enthalpy of the nonmagnetic *opv* phase becomes competitive and finally becomes the stable structure at about 880 GPa.

Experimentally,¹⁴ a post-perovskite type phase was obtained at pressure (60 GPa at 2500K) much below the one achieved here by our calculations, where the post-perovskite phase is stable with respect to the Rh₂O₃(II) phase only beyond 330 GPa. High temperature heating likely plays a role in reducing the experimental transition pressure. For instance, for the structural transition from corundum-type to Rh₂O₃(II), the transition pressure drops from 46 GPa to 26 GPa when the samples are laser heated from room temperature to about 2500K.^{11,14,15} We notice that the Cmc type post-perovskite structure proposed (without structural determination) by Ono. *et.al.*^{14,15} is never the stable one in

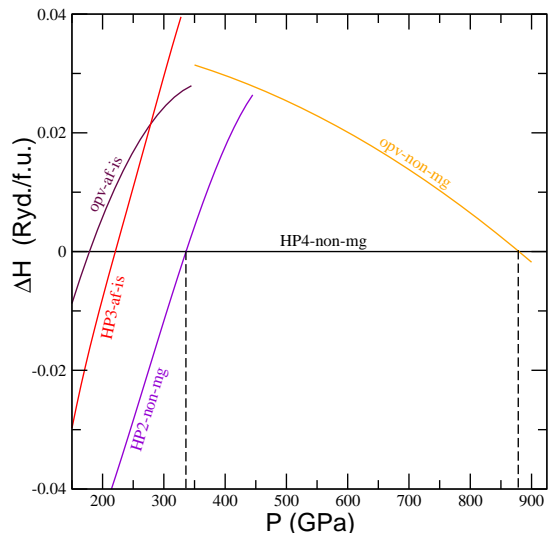


FIG. 7: (color online) Relative enthalpy curves for the Rh₂O₃(II) (HP2), *opv* (opv), Cmc type post-perovskite (HP3) and Pmc₂₁ type post-perovskite (HP4). The dashed vertical lines are guide to the eye to locate the transition pressures.

our calculations, rather Pmc₂₁ symmetry—a subgroup of Cmc—is found. Further efforts are needed to establish experimentally the structural parameters of this post-perovskite phase.

This extreme condition phase might have implications in exploring and understanding the rocky cores of solar giants and/or rocky mantles of recently discovered terrestrial exoplanets.^{36,37,38}

E. in the vicinity of spin transition and structural evolution

Before coming to conclusions we want to summarize two issues: What happens at the spin transition and what is the overall structural evolution in Fe₂O₃. We have already mentioned that the phenomena of spin transition occurs in the octahedral cages³⁹ for all the three phases that are dynamically stable at ambient pressure: *i.e.* hematite, Rh₂O₃(II) type Fe₂O₃ and Pbnm type Fe₂O₃. A vivid look into the density of states profile, depicted in Fig. 8, shows that at the transition, the *d*-band width increases substantially. Our explanation for this goes as: with increasing pressure the O atoms gets closer to the Fe atoms. This induces enhancement in the octahedral crystal field splitting of the triply degenerate *t_{2g}* and doubly degenerate *e_g* levels. At some point in the pressure scale the strength of the crystal field energy overcomes the exchange energy and the Fe atoms transit from a state with ³*t_{2g}* ²*e_g* configuration to a state with ⁵*t_{2g}* ⁰*e_g*. Also, it can be seen from Fig. 5 that in terms of magnetic state the system exists in three distinct regions, *i.e.*, with HS, LS and nonmagnetic. The transition from

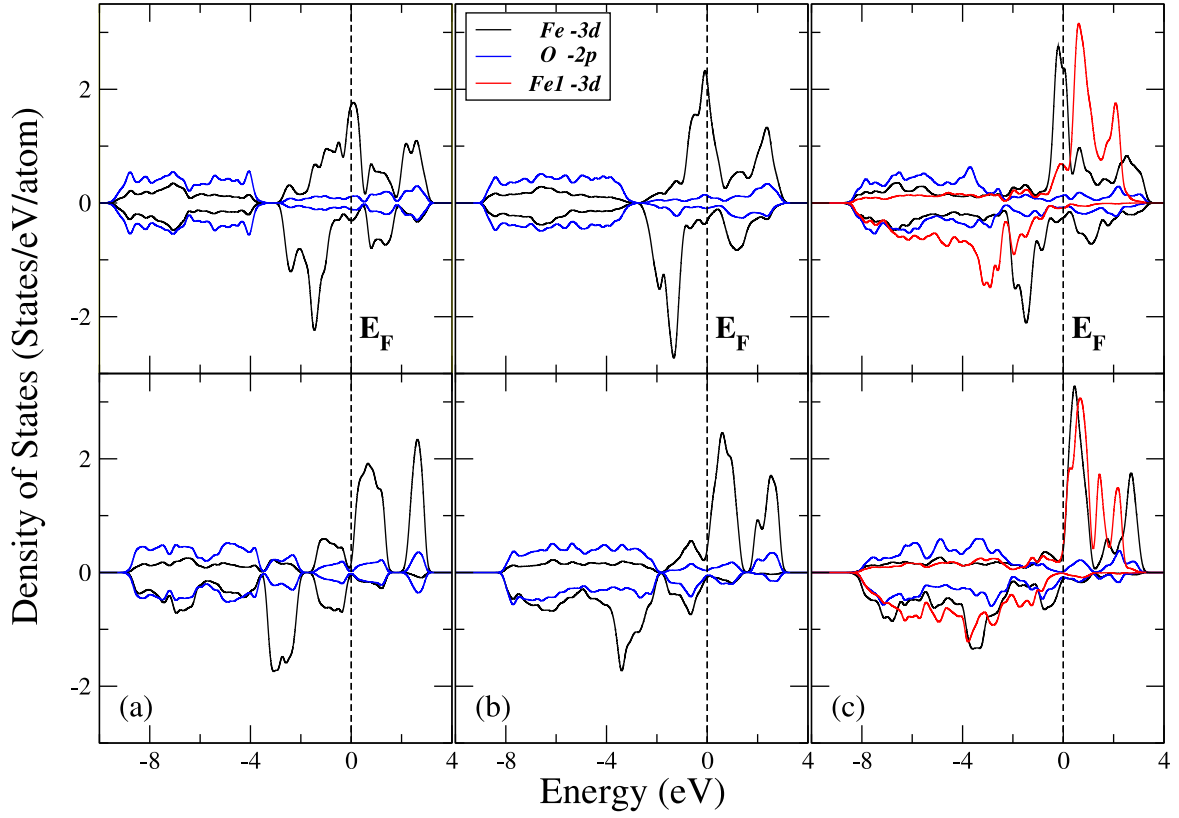


FIG. 8: (color online) Projected density of states in the vicinity of the spin transition. Lower panels show the DOS just before the spin transition occurs and the upper panels are the same just after the spin transition. (a) for the hematite structure. (b) for the $\text{Rh}_2\text{O}_3(\text{II})$ type Fe_2O_3 . (c) for the Pbnm type Fe_2O_3 . Note that in Pbnm type Fe_2O_3 Fe is in two types of polyhedral coordination. The spin transition occurs only in the octahedral cage. Whereas the Fe in 8-fold coordinated polyhedra remain in high spin.

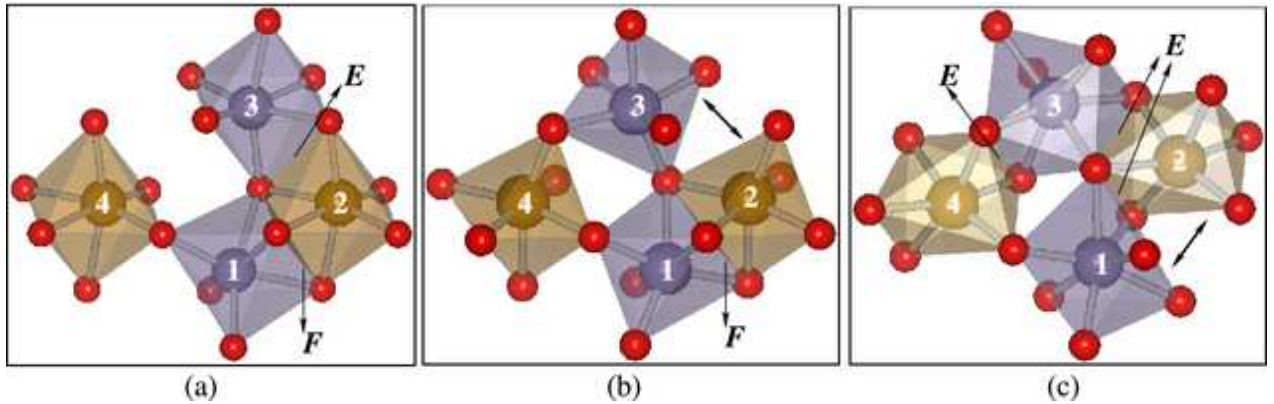


FIG. 9: (color online) Figure shows the evolution of the basic network of the polyhedra. **E** and **F** correspond respectively to edge sharing and face sharing bonding. Red (smaller) spheres are O atoms while the bigger spheres at the centres of the polyhedrons correspond to Fe atoms and are denoted by **1**, **2**, **3**, **4**. (a) correspond to Hematite, (b) $\text{Rh}_2\text{O}_3(\text{II})$ structure, and (c) $\text{Pmc}2_1$ structure. Note the changes in the edge, face and corner sharing, leading to different types of structures.

LS to the nonmagnetic state is rather gradual. This happens only when the hybridization strength between Fe-3d and O-2p levels overcomes the crystal field energy.

To explain how the structure evolves, we present the sequence of basic polyhedral network from hematite to Pmc2₁ type structure through Rh₂O₃(II) structure in Fig. 9. The face sharing network in between octahedron **1** and **2** in hematite is retained in Rh₂O₃(II). However, the edge sharing network between octahedron **2** and **3** of hematite is broken and instead a corner sharing bonding is formed between octahedron **3** and **4** in Rh₂O₃(II). In the transition from Rh₂O₃(II) to the Pmc2₁ structure, the face sharing network between octahedron **1** and **2** of Rh₂O₃(II) is broken and the rearrangement of the internal parameters leads to two kinds of polyhedral connectivity, one with 6-fold coordination (**2** and **4**) and the other with 7-fold coordination (**1** and **3**).

IV. CONCLUSION

In this work, systematic density functional calculations of Fe₂O₃ have been performed over a wide range of pressure. Corundum type phase displays high-spin to

low-spin transition for all magnetic configurations. This corundum type phase transforms to a distorted corundum or Rh₂O₃(II) type phase at about 38 GPa while Pbnm type perovskite structure don't have any stability field in this pressure regime. The phenomenon of spin transition is also present in Rh₂O₃(II) structure. On increasing pressure, our calculations identify a new structure with Pmc2₁ symmetry, a subgroup of Cmc₂, as the post-perovskite structure, while the experimentally proposed Cmc₂ phase is never the most stable one. Our calculations also show that the orthorhombic perovskite type structure with Pbnm symmetry might have a stability field at extremely high pressures.

Acknowledgments

Calculations were performed at SISSA and at CINECA computing center in Bologna, also thanks to INFM computing grants. All calculations have been done employing the PWscf code in the Quantum Espresso⁴⁰ distribution. For the graphics part VESTA⁴¹ package has been used in addition to the XCrySDen⁴² package.

-
- ¹ J. Hubbard, Proc. R. Soc. London A **277** 237 (1964).
 - ² A. F. Reid and A. E. Ringwood, J. Geophys. Res. **74** 3238 (1969).
 - ³ R. G. McQueen and S. P. Marsh, in Handbook in Physical Constants, edited by S. P. Clark, Memoir 97 of the Geological Society of America, Inc. (Geological Society of America, New York, 1966), revised ed., p. 153.
 - ⁴ R. D. Shannon and C. T. Prewitt, J. Solid State Chem. **2** 134 (1970).
 - ⁵ T. Yagi and S. Akimoto, in High Pressure Research in Geophysics, edited by S. Akimoto and M. H. Manghnani (Center Acad. Publ. Japan, Tokyo, 1982), p. 81.
 - ⁶ T. Suzuki, T. Yagi, A. Akimoto, A. Ito, S. Morimoto, and S. Syono, in Solid State Physics under Pressure, edited by S. Minomura (KTK Scientific Publishers, Tokyo, 1985), p. 149.
 - ⁷ J. Staun Olsen, C. S. G. Cousins, L. Gerward, H. Jhans, and B. J. Sheldon, Phys. Scr. **43** 327 (1991).
 - ⁸ S. Nasu, K. Kurimoto, S. Nagatomo, S. Endo, and F. E. Fujita, Hyperfine Interact. **29** 1583 (1986).
 - ⁹ Y. Syono, A. Ito, S. Morimoto, S. Suzuki, T. Yagi, and S. Akimoto, Solid State Commun. **50** 97 (1984).
 - ¹⁰ M. P. Pasternak, G. Kh. Rozenberg, G. Y. Machavariani, O. Naaman, R. D. Taylor, and R. Jeanloz, Phys. Rev. Lett. **82** 4663 (1999).
 - ¹¹ J. Badro, G. Fiquet, V. V. Struzhkin, M. Somayazulu, H.-K. Mao, G. Shen, and T. LeBihan, Phys. Rev. Lett. **89** 205504 (2002).
 - ¹² S.-H. Shim and T. S. Duffy, Am. Miner. **87** 318 (2002).
 - ¹³ G. Kh. Rozenberg, L. S. Dubrovinsky, M. P. Pasternak, O. Naaman, T. Le Bihan, and R. Ahuja, Phys. Rev. B **65** 064112 (2002).
 - ¹⁴ S. Ono, T. Kikegawa, and Y. Ohishi, J. Phys. Chem. Solids **65** 1527 (2004).
 - ¹⁵ S. Ono, K. Funakoshi, Y. Ohishi, and E. Takahashi, J. Phys.: Condens Matter **17** 269 (2005).
 - ¹⁶ G. Rollmann, A. Rohrbach, P. Entel, and J. Hafner, Phys. Rev. B **69** 165107 (2004).
 - ¹⁷ M P J Punkkinen, K Kokko, W Hergert and I J Väyrynen, J. Phys.: Condens Matter **11** 2341 (1999).
 - ¹⁸ L. M. Sandratskii, M. Uhl, and J. Kübler, J. Phys.: Condens Matter **8** 983 (1996).
 - ¹⁹ M. Catti, G. Valerio, and R. Dovesi, Phys. Rev. B **51** 7441 (1995).
 - ²⁰ J. Perdew, K. Burke, and M. Ernzerhof, Phys. Rev. Lett. **77** 3865 (1996).
 - ²¹ R. M. Wentzcovitch, Phys. Rev. B **44** 2358 (1991).
 - ²² A. M. Rappe, K. M. Rabe, E. Kaxiras and J. D. Joannopoulos, Phys. Rev. B **41** 1227 (1990).
 - ²³ H.J. Monkhorst e J.D. Pack, Phys. Rev. B **13**, 5188 (1976); J.D. Pack e H.J. Monkhorst, Phys. Rev. B **16**, 1748 (1977).
 - ²⁴ S. Mochizuki, Phys. Status Solidi A **41** 591 (1977).
 - ²⁵ J.H. Takemoto, and B. Hutchinson, Inorg. Chem. **12**, 705 (1973);
 - ²⁶ P. Gülich, Struct. Bonding, **44**, 83 (1981);
 - ²⁷ E. König, Prog. Inorg. Chem. **35**, 527 (1987);
 - ²⁸ M. Konno, and M. Mikami-kido, Bull. Chem. Soc. Jpn. **64**, 339 (1991);
 - ²⁹ N. Moliner, M.C. Munoz, S. Letard, J.-F. Letard, X. Solans, R. Burriel, M. Castro, O. Kahn, and J.-A. Real, Inorg. Chem. Acta **291**, 279 (1999).
 - ³⁰ P. Guionneau, J.-F. Letard, D.S. Yufit, D. Chasseau, G. Bravic, A.E. Goeta, J.A.K. Howard, and O. Kahn, J. Mater. Chem. **9**, 985 (1999).
 - ³¹ M. Marchivie, P. Guionneau, J.-F. Letard and D. Chasseau, Acta. Cryst. B **59**, 479 (2003).

- ³² K. Robinson, G. V. Gibbs, and P. H. Ribbe, *Science* **172** 567 (1971).
- ³³ Electronic spin transition is also observed in Pbcn and Pbnm type Fe_2O_3 . Pbnm type Fe_2O_3 has two types of polyhedral (octahedra and 8-fold coordinated polyhedra) arrangement and the electronic spin transition occurs only in the octahedra. At the spin transition the octahedral parameters jump from a higher to a lower value. See [39] for details.
- ³⁴ J. Tsuchiya, T. Tsuchiya, and R. M. Wentzcovitch, *Phys. Rev. B* **72** 020103(R) (2005).
- ³⁵ Here as a note we want to mention that with increasing pressure the HP3 phase shows instability in convergence. Umemoto *et. al.*⁴³ showed that in Cmcn type NaMgF_3 there is softening of zone edge frequency at Y-point with increasing pressure. The structural relaxation after atomic displacements lead to the Pmcn type U_2S_3 structure after the Cmcn type structure in NaMgF_3 . In our calculations we have put some atomic displacements to the structure in the HP3 phase and then relaxed the structure. This lead to this new structure which is dynamically stable down to 100 GPa. This might be indicative that this structural phase transition is not due to softening of any frequency mode, but it's a pressure induced enthalpy driven one.
- ³⁶ T. Guillot, *Phys. Today* **57** 63-69 (2004).
- ³⁷ E. J. Rivera et al., *Astrophys. J.* **634** 625 (2005).
- ³⁸ D. Valencia, R. J. OConnell, D. Sasselo, *Icarus* **181** 545-554 (2006).
- ³⁹ D. B. Ghosh, and S. de Gironcoli, communicated to *Phys. Rev. B*.
- ⁴⁰ <http://www.pwscf.org>
- ⁴¹ K. Momma and F. Izumi, *Commission on Crystallogr. Comput., IUCr Newslett.*, **7** 106-119 (2006).
- ⁴² <http://www.xcrysden.org>
- ⁴³ K. Umemoto and R. M. Wentzcovitch, *Phys. Rev. B* **74** 224105 (2006).